Central Washington University

ScholarWorks@CWU

All Faculty Scholarship for the College of the Sciences

College of the Sciences

10-31-2019

Tools for Prescreening the Most Active Sites on Ir and Rh Clusters toward C–H Bond Cleavage of Ethane: NBO Charges and Wiberg Bond Indexes

Yingbin Ge
Central Washington University

Anna Le
Central Washington University

Gregory J. Marquino
Central Washington University

Phuc Q. Nguyen
Central Washington University

Kollin Trujillo
Central Washington University

See next page for additional authors

Follow this and additional works at: https://digitalcommons.cwu.edu/cotsfac

Part of the Chemistry Commons

Recommended Citation

Ge, Yingbin; Le, Anna; Marquino, Gregory J.; Nguyen, Phuc Q.; Trujillo, Kollin; Schimelfenig, Morgan; and Noble, Ashley, "Tools for Prescreening the Most Active Sites on Ir and Rh Clusters toward C–H Bond Cleavage of Ethane: NBO Charges and Wiberg Bond Indexes" (2019). *All Faculty Scholarship for the College of the Sciences*. 95.
https://digitalcommons.cwu.edu/cotsfac/95

This Article is brought to you for free and open access by the College of the Sciences at ScholarWorks@CWU. It has been accepted for inclusion in All Faculty Scholarship for the College of the Sciences by an authorized administrator of ScholarWorks@CWU. For more information, please contact scholarworks@cwu.edu.

Authors

Yingbin Ge, Anna Le, Gregory J. Marquino, Phuc Q. Nguyen, Kollin Trujillo, Morgan Schimelfenig, and Ashley Noble

This article is available at ScholarWorks@CWU: https://digitalcommons.cwu.edu/cotsfac/95

This is an open access article published under a Creative Commons Attribution (CC-BY) License, which permits unrestricted use, distribution and reproduction in any medium, provided the author and source are cited.

ACS OMEGA

Article

Cite This: ACS Omega 2019, 4, 18809−18819

http://pubs.acs.org/journal/acsodf

Tools for Prescreening the Most Active Sites on Ir and Rh Clusters toward C−H Bond Cleavage of Ethane: NBO Charges and Wiberg Bond Indexes

Yingbin Ge,* Anna Le, Gregory J. Marquino, Phuc Q. Nguyen, Kollin Trujillo, Morgan Schimelfenig, and Ashley Noble

Department of Chemistry, Central Washington University, Ellensburg, Washington 98926, United States

Supporting Information

ABSTRACT: B3LYP calculations were carried out to study the insertion of iridium (Ir) and rhodium (Rh) clusters into a C−H bond of ethane, which is often the rate-limiting step of the catalytic cycle of oxidative dehydrogenation of ethane. Our previous research on Ir catalysis correlates the diffusivity of the lowest unoccupied molecular orbital of the Ir clusters and the relative activities of the various catalytic sites. The drawback of this research is that the molecular orbital visualization is qualitative rather than quantitative. Therefore, in this study on C−H bond activation by the Ir and Rh clusters, we conducted analyses of natural bond orbital (NBO) charges and Wiberg bond indexes (WBIs), both of which are not only quantitative but also independent of the basis sets. We found strong correlation between the NBO charges, the WBIs, and the relative activities of the various catalytic sites on the Ir and Rh clusters. Analyses of the NBO charges and the WBIs provide a fast and reliable means of prescreening the most active sites on the Ir and Rh clusters and potentially on other similar transition-metal clusters that activate the C−H bonds of ethane and other light alkanes.

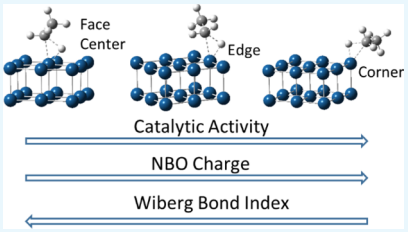

INTRODUCTION

Catalyzed dehydrogenation of alkanes is an important petroleum industrial process. Approximately 134 million tons of ethene (ethylene) and 94 million tons of propene (propylene) were produced in 2014.[1,2] These numbers are expected to increase continuously as the consumption of ethene and propene is expected to increase continuously. Consequently, transition-metal (TM) catalysts used for the dehydrogenation of ethane and other light alkanes have been extensively studied both experimentally and theoretically.[3−29] The energy consumption for converting alkanes to alkenes is tremendous because it takes more than 400 kJ/mol of energy to break a C−H bond. Although the traditional vanadium oxide catalysts can reduce the energy barrier of the oxidative dehydrogenation (ODH) of alkanes to 100−200 kJ/mol,[5,27−29] a high-temperature environment is still required to provide enough thermal energy for this catalyzed reaction. More effective TM catalysts are desirable for the mass production of ethene and propene at a lower energy cost.

Recently, platinum (Pt) atomic clusters were found to have an extraordinary ability to break C−H bonds at lower temperatures by reducing the energy barrier to ∼20 kJ/mol, both in the gas phase and on a metal oxide surface.[6,7] This is a breakthrough toward the catalysis of the ODH of alkanes. However, Pt clusters can easily coalesce in the gas phase and lose their catalytic activity. When they are supported by a metal oxide surface, coalescence may still occur at high reaction temperatures.[30,31] Similar catalytic abilities and shortcomings are observed for several other TM clusters. Iridium (Ir), rhodium (Rh), and palladium (Pd) atomic clusters have shown tremendous potential toward activating the C−H bonds of ethane and propane, both in the gas phase and on metal oxide surfaces.[12−19] However, studies also show that small TM clusters such as Ir_3 migrate easily on metal oxide surfaces.[32] Apart from enhancing the catalytic ability of these TM clusters, preventing their migration, coalescence, and deactivation are equally important. One strategy we proposed in a previous study was to find catalytically active Ir clusters with large enough surfaces that can bond strongly to their support to hinder migration.[16]

In our previous research,[16] the ODH of ethane and propane catalyzed by the Ir_8, Ir_{12}, and Ir_{18} atomic clusters was investigated. The reaction cycle of the Ir cluster-catalyzed ODH of ethane involves five steps, as shown in Figure 1: first, C_2H_6 approaches an Ir_n cluster to form the $Ir_n\cdots C_2H_6$ reactant complex. Second, the Ir_n cluster enters a C−H bond of ethane and forms $H-Ir_n-C_2H_5$. This was found to be the rate-limiting step. Third, the Ir_n cluster enters a second C−H bond and forms $(H)_2-Ir_n-C_2H_4$, in which ethylene is formed and bonded to Ir_n. The formation of the C−C π bond facilitates the second H elimination. Fourth, O_2 is adsorbed on the Ir_n surface and decomposed into two O atoms, each bonded to the Ir_n cluster. The H atoms migrate on the Ir cluster until encountering an O atom. O−H bonds and eventually H_2O are

Received: August 31, 2019
Accepted: October 18, 2019
Published: October 31, 2019

© 2019 American Chemical Society

DOI: 10.1021/acsomega.9b02813
ACS Omega 2019, 4, 18809−18819

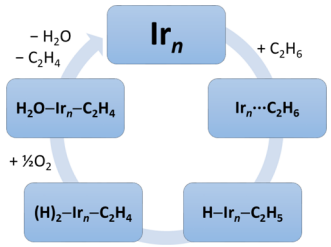

Figure 1. Reaction cycle of the Ir_n cluster-catalyzed ODH of ethane.

formed and heat is released. Fifth, water and ethylene are evaporated from the Ir_n surface assisted by the heat released from the formation of the O–H bonds.

We had chosen Ir_8, Ir_{12}, and Ir_{18} atomic clusters to model this catalytic cycle for two reasons:[16] first, CCSD(T) and density functional theory (DFT) calculations predicted that the global minimum structures of these Ir atomic clusters adopt a cubic or cuboid shape.[33,34] These predictions provided a starting point for us to focus on the modeling of these cubic/cuboid structures of Ir clusters and their activities toward ethane and propane. Second, these cubic or cuboid structures may have up to half of the Ir atoms (4, 6, or 9) bonded to a supporting surface, which may reduce their chances of migrating on the surfaces compared with the much smaller Ir clusters such as Ir_3.[32]

It was straightforward to study the insertion of Ir_8 clusters into a C–H bond of ethane because all Ir atoms are identical in the Ir_8 cube. There are, however, two types of atoms in the 3 cube. 2 cuboid structure of Ir_{12}: eight atoms on the corner sites and four on the edges. In the 3 × 3 × 2 cuboid structure of Ir_{18}, there are corner, edge, and face center sites. In total, we studied six different reaction paths of Ir_n (n = 8, 12, and 18) interacting with ethane on various catalytic sites.[16] The six corresponding transition-state (TS) structures are illustrated in Figure 2. Because of the many nearly degenerate electronic structures of the Ir_n clusters, we computed each reaction path in at least seven electronic states with the electron spin quantum number (S) ranging from 0 to 6. The reaction path with the lowest energy barrier was then used to characterize the activity of the cluster size and the catalytic site of interest.[16] We found that the catalytic ability of the Ir clusters depends both on the cluster size and on the catalytic site. The corner sites of Ir_{18} ($\Delta H^{\ddagger}$ = 3 kJ/mol) are more active than the corner sites of Ir_{12} ($\Delta H^{\ddagger}$ = 21 kJ/mol) and Ir_8 ($\Delta H^{\ddagger}$ = 65 kJ/mol). Because the Mulliken analysis suggests that electrons flow from ethane to the Ir_n cluster in the $Ir_n + C_2H_6 \rightarrow H–Ir_n–C_2H_5$ reaction, we conjectured that larger Ir clusters disperse the negative charge better than the smaller ones and thus stabilize the TS. The molecular orbital (MO) visualization shows that the lowest unoccupied MOs (LUMOs) are more diffuse at the corner sites and thereby more readily accept the C–H bonding electrons. The LUMOs are tighter at the edge sites and the tightest at the face center sites. Consequently, the corner sites are more active than the edge sites, which are in turn more active than the face center sites. For example, the enthalpy of activation ($\Delta H^{\ddagger}$) of $Ir_{18} + C_2H_6 \rightarrow H–Ir_{18}–C_2H_5$ is 3, 48, or 71 kJ/mol at the corner, edge, or face center site, respectively.

The Mulliken analysis and the visualization of MOs supported our explanation of the size and site effects on the catalytic abilities of Ir clusters.[16] However, these two means are rather qualitative and dependent on the basis sets. The MO visualization also depends on the isovalues chosen for the MO graphing. Therefore, quantitative indicators that are independent of basis sets, such as natural bond orbital (NBO) charges[35,36] and Wiberg bond indexes (WBIs),[37−39] are desirable for predicting the activity of the various catalytic sites.

In this paper, we conducted the NBO charge and WBI analyses for the previously studied Ir clusters. We then extended these analyses to the Rh_n clusters that catalyze the dehydrogenation of ethane. Rh and Ir are both group 9 TM elements. Rh is in the fifth period and Ir is in the sixth. Because of the lanthanide contraction, Rh and Ir have a similar atomic radius (~1.34 Å vs ~1.36 Å). However, Rh and Ir clusters may behave differently in their reactions with ethane because the Rh and Ir atoms have different electronic structures. The Rh atom has a $[^{36}Kr]4d^8 5s^1$ electronic configuration, notably different from the $[^{54}Xe]4f^{14}5d^7 6s^2$ configuration of Ir in the numbers of the valence d and s electrons. Finding the lowest-energy structures of the Rh clusters becomes the first considerable challenge before we can study their catalytic behaviors. The results of the global optimization heavily depend on the computational methods used to model the Rh clusters. For example, Lecours et al.[40] searched for the global minimum structures of Rh_{n+1}^+ and Rh_nS^+ using the Perdew–Burke–Ernzerhof (PBE)[41] and PBE0[42] generalized gradient

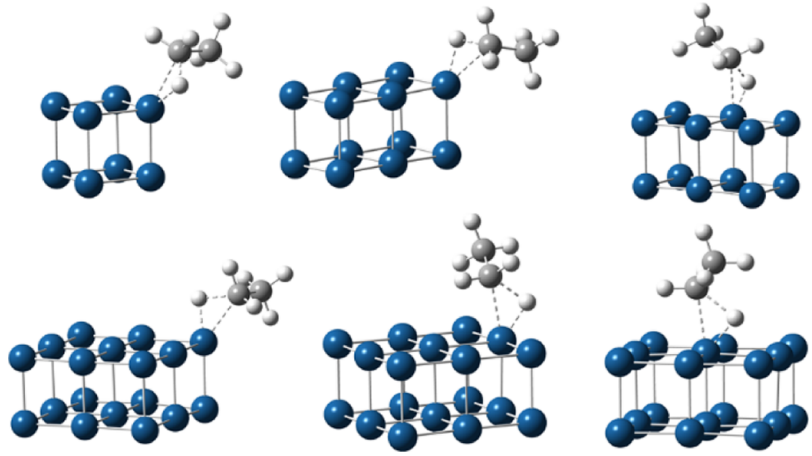

Figure 2. Previously studied TS structures of $Ir_n + C_2H_6 \rightarrow H–Ir_n–C_2H_5$ reaction taking place at the corner, edge, and/or face center sites of the Ir_8, Ir_{12}, Ir_{18} cubic, or cuboid structures with the electron spin quantum number S ranging from 0 to 6.

DOI: 10.1021/acsomega.9b02813
ACS Omega 2019, 4, 18809−18819

approximation (GGA) method. The PBE pure GGA calculations suggest a cubic lowest-energy structure for Rh_8^+ with an electron spin number (S) of 8, whereas the PBE0 hybrid GGA calculations suggest a bicapped octahedron structure with a C_{2v} point group and S = 14.[40] The PBE0 results differ from the PBE results drastically for other Rh species as well.[40] Which method, or which category of the DFT methods (e.g., hybrid vs pure GGA), is more accurate for modeling the Rh clusters? This question prompted us to assess the accuracy of various DFT methods in the next section before eventually choosing the B3LYP hybrid GGA method for the study of the Rh clusters and their interaction with ethane.

Other than the method selection, there is another issue that hinders a comprehensive study of the catalytic activities of the Rh clusters. Unlike the previous Ir study[16] in which we knew Ir_{18} prefers a cuboid structure that contains only three different catalytic sites, the Rh_{18} clusters may adopt less symmetrical structures, each with a larger number of unique catalytic sites. This poses a grave challenge in the study of the Rh_{18} clusters as we learned that the catalytic activity of a TM cluster may heavily depend on the reaction site.[16] Figure 3 illustrates how

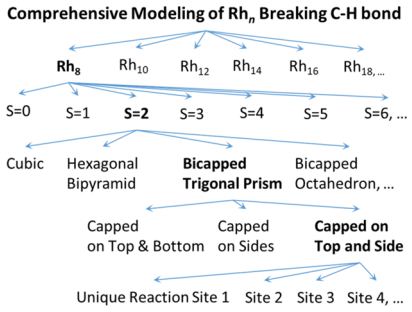

Figure 3. Flow chart of a comprehensive modeling of the $Rh_n + C_2H_6 \rightarrow H{-}Rh_n{-}C_2H_5$ reaction.

complicated the study on Rh catalysis can be. We need to study various cluster sizes. For each size, we need to find the lowest energy structures, including their electron spin quantum numbers. We then need to study all different catalytic sites for each of these lowest-energy structures—this task is much more daunting for many other less symmetrical atomic structures of the larger Rh clusters. A fast and reliable method of prescreening the various catalytic sites is desirable to make a comprehensive study on Rh catalysis feasible.

In this paper, we first carried out the NBO[35,36] calculations for the Ir_8, Ir_{12}, and Ir_{18} clusters. The NBO charges correlate strongly with the activities of the various catalytic sites. Equally, or even more strongly than the NBO charges, the WBIs[37−39] of the Ir atoms at different sites correlate with their activities toward the dehydrogenation of ethane. We then extended these analyses to similar Rh clusters and found similar correlations. These findings may result in a fast and reliable means of prescreening the catalytic sites of the Ir_n and Rh_n clusters and potentially other similar TM clusters that activate the C−H bonds of alkanes.

In the next section, we introduce the computational methods chosen for this study and justify our choice. In the Results and Discussion section, we present the strong correlations between the NBO charges, the WBIs, and the catalytic ability of the various sites on the Ir and Rh clusters. Concluding remarks are given at the end.

COMPUTATIONAL METHODS

The B3LYP hybrid GGA method[43−45] implemented in Gaussian 09[46] was used in this study. The D3 empirical dispersion formulated by Grimme with Becke−Johnson damping[47] (D3BJ) was included in all calculations. In the geometry optimization and vibrational frequency calculations, polarized double-ζ (DZ) basis sets were used. The LANL2DZ basis set and the LANL2 effective core potential,[48] augmented with f-type polarization functions,[49] were employed on the Rh atoms. The 6-31G(d) basis sets were employed on the C, H, and O atoms.[50,51] This computing scheme is similar to Liu et al.'s calculations on the functionalization of C−H bonds,[52] Yang et al.'s calculations on the C−H activation by Rh complexes,[53] and Karmel et al.'s calculations on the Rh-catalyzed silylation of alkyl C−H bonds.[54] The only difference is that we also included the f-type polarization functions on the Rh atoms for enhanced accuracy. Similarly, Sundermann et al. studied C−C and C−H activation by Rh complexes using the B3LYP/LANL2DZ+p method.[55] DeAngelis et al. studied the Rh-complex-catalyzed C−H functionalization of indoles using B3LYP calculations with the 6-311G(d,p) basis sets on main group elements and LANL2DZ on Rh.[56] In a recent article on the assessment of DFT studies of Rh-mediated chemical transformations, the inclusion of the D3 empirical dispersion is shown to be important.[57] While PBE0 and MPWB1K-D3 are found to be the most accurate methods for the test cases used in this article,[57] the B3LYP-D3 method is reasonably accurate and clearly outperform B3LYP. Our choice of the B3LYP-D3BJ method was partially justified by these previous studies on the Rh-containing systems.

In addition to the literature review, we assessed several categories of the DFT methods before eventually choosing the B3LYP hybrid GGA method for this study. Figure 4 shows the comparison between eight popular DFT methods—all coupled

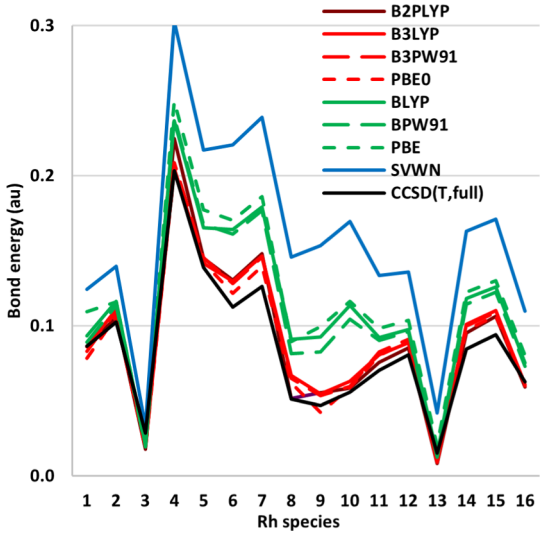

Figure 4. Rh−X (X = H, C, O, and Rh) bond energies of small Rh species: the DFT results vs the benchmark CCSD(T, full) results. The four categories of the double-hybrid, hybrid GGA, pure GGA, and local DFT calculations are colored purple, red, green, and blue, respectively. The benchmark is in black color. Species 1−16 are ^{1}RhH, ^{3}RhH, ^{5}RhH, ^{2}RhC, ^{4}RhC, ^{2}RhO, ^{4}RhO, $^1Rh_2$, $^3Rh_2$, $^5Rh_2$, $^1RhCH_3$, $^3RhCH_3$, $^5RhCH_3$, ^{1}RhOH, ^{3}RhOH, and ^{5}RhOH, respectively.

DOI: 10.1021/acsomega.9b02813
ACS Omega 2019, 4, 18809−18819

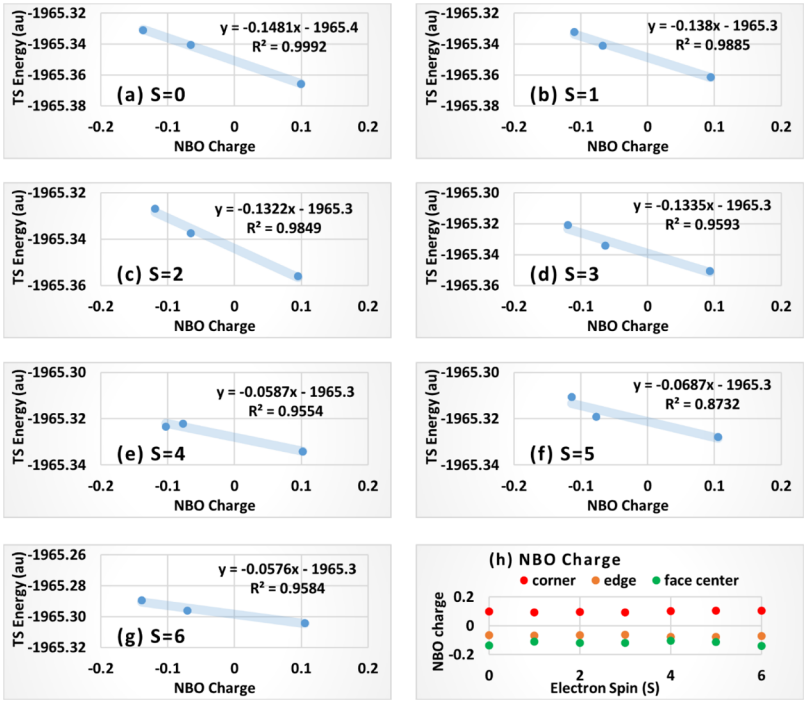

Figure 5. (a–g) Electron spin S = 0–6: Correlation between the TS energy of the Ir_{18} + C_2H_6 → H–Ir_{18}–C_2H_5 reaction and the NBO charges of the face center, edge, and corner (from left to right) catalytic sites of Ir_{18}. (h) NBO charges of the three catalytic sites of Ir_{18} (S = 0–6).

with the D3BJ empirical dispersion—against the CCSD(T, full) benchmark calculations of the bond energies of small Rh species. The assessed DFT methods include the double-hybrid B2PLYP[58] with HF exchange and MP2-type correlation (purple color), the B3LYP,[43−45] B3PW91,[43,59−62] and PBE0[42] hybrid GGA methods with HF exchange (red color), the BLYP,[44,63] BPW91,[59,60,63] and PBE[41] pure GGA methods (green color), and the SVWN[64−67] local method (black color). The B3LYP, B3PW91, and PBE0 hybrid GGA methods differ from the BLYP, BPW91, PBE pure GGA method mainly in their inclusion of 20% (B3) or 25% (PBE0) Hartree–Fock exchange energy. The bond energies of 16 Rh species, ^{1}RhH, ^{3}RhH, ^{5}RhH, ^{2}RhC, ^{4}RhC, ^{2}RhO, ^{4}RhO, $^1Rh_2$, $^3Rh_2$, $^5Rh_2$, $^1RhCH_3$, $^3RhCH_3$, $^5RhCH_3$, ^{1}RhOH, ^{3}RhOH, and ^{5}RhOH, were calculated. The numeric superscripts in front of these formulas are the spin multiplicities (M = 2S + 1), where S is the electron spin quantum number. The triple-ζ (TZ) LANL2TZ(f) basis set on the Rh atoms[48,49,68] and the 6-311G(d,p) basis sets on the light atoms[69] were used consistently in the DFT and CCSD(T, full) calculations. Figure 4 shows that the double-hybrid B2PLYP method and the hybrid GGA methods clearly outperform the pure GGA methods and the local SVWN method. Practical consideration of the limited computing resources ruled out the double-hybrid B2PLYP method because computing the MP2-type correlation is prohibitively expensive for larger Rh clusters. Our earlier research on the Ir_n-catalyzed dehydrogenation of ethane and propane[19] also justified the choice of using the B3LYP hybrid GGA method for this study.

The B3LYP-D3BJ frequency calculations ensured that all local minima have zero imaginary frequencies, whereas all TS structures have one imaginary frequency. Intrinsic reaction coordinate calculations were carried out to ensure that each TS connects the desired reactant (i.e., the Rh_n···C_2H_6 reactant complex) and product (i.e., H–Rh_n–C_2H_5) via the minimum energy path of the imaginary frequency. To further improve the accuracy of the thermochemistry of the Rh_n-activated C–H bond cleavage of ethane, single-point energies were calculated using polarized TZ basis sets. The LANL2TZ(f) basis set[48,49,68] was employed on the Rh atoms and the 6-311G(d,p) basis sets on the light atoms.[69] The NBO charges and the WBIs were obtained via using the same computational schemes. The NBO analysis was carried out using version 3.1 of the NBO program[70] implemented in Gaussian 09.[46]

RESULTS AND DISCUSSION

Two mechanisms account for inserting a TM atom into a C–H bond: (1) the C–H bonding electrons flow into empty d orbitals of the TM atom. (2) The d-electrons of the TM atom flow into the empty σ* C–H antibonding orbital. The Mulliken charge analysis showed that the first mechanism accounts for the Ir-activated C–H bond breaking.[16] However, this is not conclusive as the Mulliken population analysis depends heavily on the basis sets.[71−73] Therefore, in this paper, we computed the NBO charges, which are generally independent of the basis sets.[72,73] The NBO charge analysis agrees with the previous Mulliken charge analysis that C–H bonding electrons flow into the partially empty d orbitals of the Ir clusters. In the previous research, we found that the LUMO of the Ir_n clusters are much more diffuse on the corner sites and thus better overlap with the C–H σ bonding orbital.[16] In this study, we observed similar shapes of the LUMOs of the Rh clusters: The part of the LUMO around the corner site of Rh_{18} appears more diffuse than that around the edge and face center sites. As a result, the corner sites are the most active: the enthalpies of activation ($\Delta H^{\ddagger}$) of Rh_{18} + C_2H_6 → H–Rh_{18}–C_2H_5 are 0, 20, and 32 kJ/mol on the corner, edge, and face center site, respectively. The zero $\Delta H^{\ddagger}$ at the corner site is due to the fortuitous and complete cancellation between the enthalpy decrease in the formation of the Rh_{18}···C_2H_6 reactant

DOI: 10.1021/acsomega.9b02813
ACS Omega 2019, 4, 18809−18819

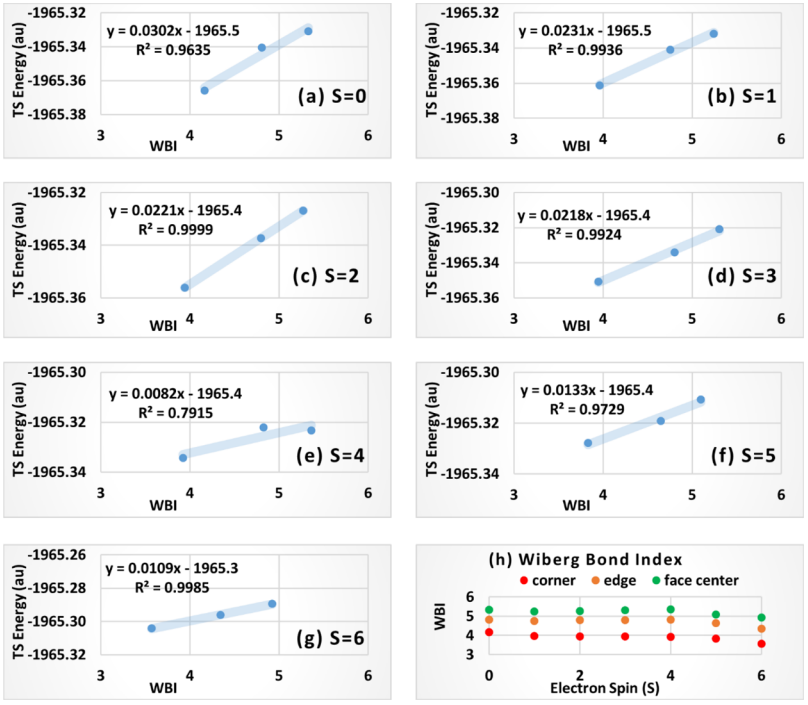

Figure 6. (a–g) Electron spin S = 0–6: Correlation between the TS energy of the Ir_{18} + C_2H_6 → H–Ir_{18}–C_2H_5 reaction and the WBIs of the corner, edge, and face center (from left to right) catalytic sites of Ir_{18}. (h) WBIs of the three catalytic sites of Ir_{18} (S = 0–6).

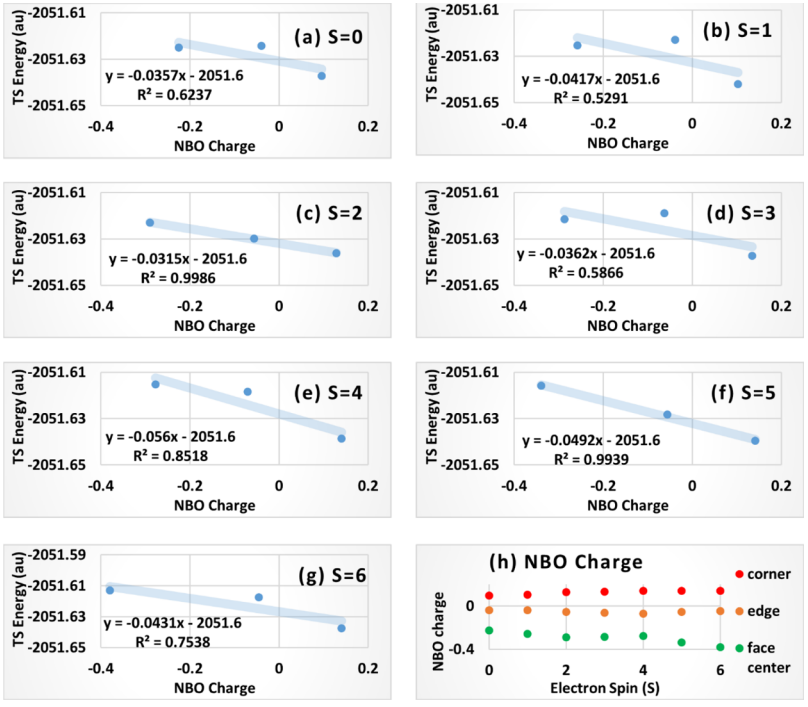

Figure 7. (a–g) Electron spin S = 0–6: Correlation between the TS energy of the Rh_{18} + C_2H_6 → H–Rh_{18}–C_2H_5 reaction and the NBO charges of the face center, edge, and corner (from left to right) catalytic sites of Rh_{18}. (h) NBO charges of the three catalytic sites of Rh_{18} (S = 0–6).

complex and the enthalpy increase in the formation of TS from the reactant complex. This trend of the Rh_{18} catalysis is similar to that of the Ir_{18} catalysis: $\Delta H^{\ddagger}$ = 3, 48, and 71 kJ/mol on the corner, edge, and face center sites, respectively, as Ir_{18} enters a C–H bond of ethane.[16] The prominent site effects of the Rh and Ir catalysis can be explained by the MO visualization. The drawbacks of the MO visualization are, however, that the shapes of the MOs depend on the isovalues chosen for graphing and that the MO visualization is rather qualitative. Therefore, in addition to the MO visualization, we studied the correlations between the TS energy (in atomic unit or au) of the TM_n + C_2H_6 → H–TM_n–C_2H_5 reactions and two quantitative indicators: NBO charges and WBIs on the corner, edge, and face center sites. The TS energy is a quantitative indicator of the catalytic activity: the more negative the TS energy is, the more active the TM cluster is. Figures 5–8

DOI: 10.1021/acsomega.9b02813
ACS Omega 2019, 4, 18809–18819

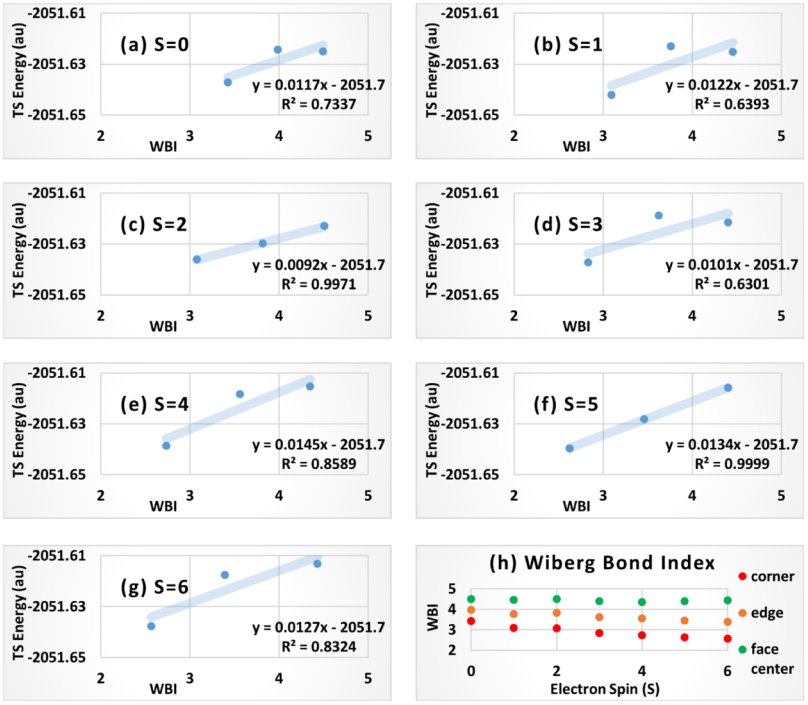

Figure 8. (a–g) Electron spin S = 0–6: Correlation between the TS energy of the $Rh_{18} + C_2H_6 \rightarrow H{-}Rh_{18}{-}C_2H_5$ reaction and the WBIs of the corner, edge, and face center (from left to right) catalytic sites of Rh_{18}. (h) WBIs of the three catalytic sites of Rh_{18} (S = 0–6).

show the strong correlations between the NBO charges, the WBIs, and the activities of the various catalytic sites of Ir and Rh clusters.

The NBO charges of the various catalytic sites of Ir_{18} correlate strongly with their activities toward the C–H bonds of ethane. Figure 5a–g shows that the TS energy for the $Ir_{18} + C_2H_6 \rightarrow H{-}Ir_{18}{-}C_2H_5$ reaction occurring at the corner, edge, and face center sites is linear to the NBO charges on these sites. This nearly perfect linear correlation is observed for each of the seven electron spin quantum number (S = 0–6). The R^2 values (a.k.a., coefficient of determination) range from 0.873 (S = 5) to 0.999 (S = 0) with an average of 0.960. Figure 5h clearly shows that, regardless of the electron spin, the corner sites are consistently positively charged, while the edge and face center sites are consistently negatively charged. The positive charge on the corner sites makes it easier for the electrons to flow from the C–H bonding orbital to the Ir clusters. For the seven reaction paths each with a different electron spin number S from 0 to 6, the spin-averaged NBO charges of the corner, edge, and face center sites of the free Ir_{18} cluster are 0.10 ± 0.01, −0.07 ± 0.01, and −0.12 ± 0.01, respectively. The spin-averaged NBO charges on these sites become −0.26 ± 0.01, −0.39 ± 0.03, and −0.45 ± 0.01 in the corresponding TS structures. The net changes of the NBO charge of the Ir atoms are −0.36, −0.32, and −0.33. The NBO charge analysis confirms that electrons flow from the C–H σ bonding orbital to the activating Ir atom, and the positively charged Ir atoms at the corner sites accept the electron more readily.

In addition to the NBO charges, the WBIs of the corner, edge, and face center atoms are also strong indicators of their ability to enter a C–H bond. Herein, the WBI of a catalytic site (or a TM atom) refers to the sum of the WBI values of all the links of the site (or atom), unless specified otherwise. Figure 6a–g shows a clear trend: The lower the WBI of the catalytic site, the lower the corresponding TS energy, and thus the more active the site. The R^2 values range from 0.791 (S = 4) to 1.000 (S = 2) with an average of 0.959. Figure 6h shows that the corner site has consistently lower WBI than the edge and face center sites, which suggests that the corner Ir atoms are the least coordinated in the Ir_{18} cuboid structures. Because of their severe undercoordination, the corner sites are more likely electron-deficient and therefore more likely to accept electrons from the C–H bonding orbital of ethane. Figures 5 and 6 show that, prior to finding the TS structures, we can rank the activities of the corner, edge, and face center site, quantitatively, solely based on the NBO charges and WBI of these sites in the Ir_n clusters. This could have saved tremendous amount of computing time in the study of Ir catalysis. For example, the efficiency of finding the lowest-energy path of Ir_{18}-catalyzed dehydrogenation of ethane would have increased 3-fold, had we known that the most positively charged corner sites with the lowest WBIs would be the most active sites and thus omitted the edge and face center sites.

Besides the WBIs of the catalytic sites, the WBIs of the Ir–C partial bond in the TS structure also strongly correlate with the TS energy. The greater the Ir–C WBI, the lower the TS energy. The Ir–C WBI serves as another useful indicator of the catalytic activity. Its value can be determined, however, only after the TS structure is optimized. In contrast, the WBIs of the catalytic sites on the Ir atomic clusters can serve as a prescreening tool before the TS structure is obtained. Similarly, the Rh–C WBIs correlate well with the corresponding TS energies (with one exception when S = 1) but cannot serve as a prescreening tool like the WBIs of the sites on the Rh atomic clusters. For more detail, the 14 plots of TS energy versus the Ir–C (or Rh–C) WBI for Ir_{18} and Rh_{18} (S = 0–6) are included in Appendix E of the Supporting Information.

We then extended the NBO charge analysis to the Rh_{18} clusters. The correlation between the NBO charges on the

DOI: 10.1021/acsomega.9b02813
ACS Omega 2019, 4, 18809–18819

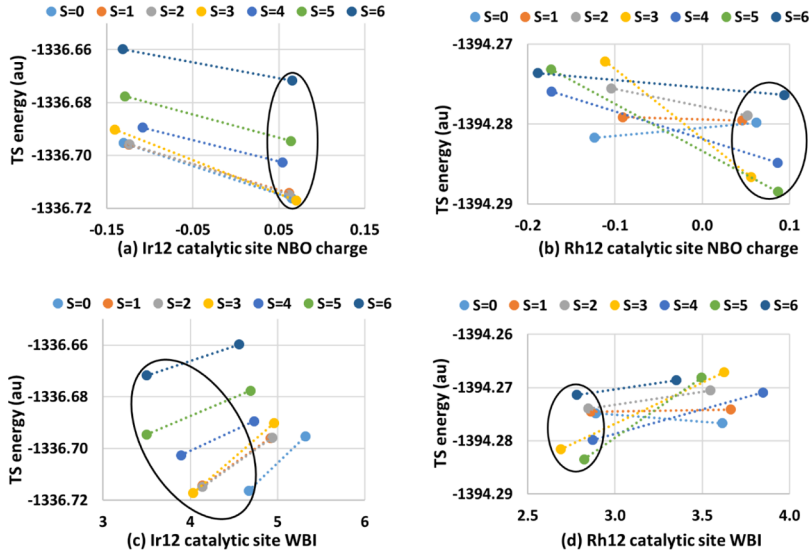

Figure 9. (a,b) Correlation between the TS energy of $TM_{12} + C_2H_6 \rightarrow H-TM_{12}-C_2H_5$ (TM = Ir and Rh) and the NBO charges of the corner and edge catalytic sites (S = 0−6). (c,d) Correlation between the TS energy and the WBIs at the corner and edge catalytic sites of the Ir_{12} and Rh_{12} cuboid structures. Enclosed in the ellipses are the corner site data.

corner, edge, and face center sites and the TS energies of Rh_{18} is weaker than Ir_{18} but still quite prominent (Figure 7). The R^2 values range from 0.529 (S = 1) to 0.999 (S = 2) with an average value of 0.763. The weaker correlation mainly results from the TS energy of the edge site being slightly higher (instead of lower) than that of the face center site, when S = 0, 1, or 3. However, the corner site consistently has the most positive NBO charge and the lowest TS energy, which makes the NBO charge of the free Rh_n cluster a useful indicator for finding the most active sites. The NBO charges of the corner, edge, and face center sites of the free Rh_{18} cluster are 0.13 ± 0.02, −0.05 ± 0.01, and −0.29 ± 0.05. The NBO charges on the corresponding sites become −0.22 ± 0.01, −0.35 ± 0.03, and −0.61 ± 0.01 in the TS structures. The net changes of the NBO charge of the Rh atoms are −0.35, −0.30, and −0.32 as the Rh atoms at the corner, edge, and face center sites enter a C−H bond of ethane. Similar to the Ir_{18} analysis, we found that electrons flow from the C−H σ bonding orbital to the activating Rh atom and that the positively charged Rh atoms at the corner sites accept the electron more readily. This explains why the corner sites weaken the C−H bonds of ethane more efficiently than the edge and face center sites.

Figure 8a−g shows that the WBIs act as a slightly better indicator than the NBO charges for the Rh_{18} case. The R^2 values range from 0.630 (S = 3) to 1.000 (S = 5) with an average of 0.813. Although exceptions to the linear relationships were found for the S = 0, S = 1, and S = 3 cases, the corner sites have the lowest WBIs and also the lowest TS energies consistently for each spin (S = 0−6). Figure 8h shows that the corner sites always have the lowest WBIs, followed by the edge and face center sites, in that order. As anticipated, the most severely undercoordinated corner sites interact with the C−H bonds more strongly, which lowers the TS energy of the reaction taking place on the corner site. Collectively, Figures 5−8 suggest that the NBO and WBI analyses are excellent prescreening tools for ranking the catalytic sites in both Ir_{18} and Rh_{18}. The corner sites always have the most positive NBO charges, the lowest WBIs, and the strongest activities toward the C−H bonds of ethane.

How do the NBO and WBI analyses work for the Ir and Rh clusters with a different size such as Ir_{12} and Rh_{12}? Because the Ir_{12} and Rh_{12} clusters have only two different sites (corner and edge), we pooled the correlations (S = 0−6) between the NBO charges and the TS energy of Ir_{12} in Figure 9a and that of Rh_{12} in Figure 9b. Figure 9a for Ir_{12} exhibits similar "TS energy versus NBO charge" slopes for all seven electron spin numbers from 0 to 6. The correlation for Rh_{12} is also prominent but weaker than Ir_{12} especially for the S = 0 case, in which the edge site with a negative NBO charge has lower (instead of higher) TS energy than the corner site with a positive charge. Figure 9c,d shows that a lower WBI is still an excellent indicator of the stronger catalytic ability for the Ir_{12} clusters for each electron spin. There is again an exception (S = 0) for the Rh_{12} case, but overall, the WBI correlates strongly with the catalytic ability of the corner and edge sites of Rh_{12}. In summary, Figures 5−9 suggest that the NBO charge and WBI analyses rank the catalytic sites accurately for both Ir and Rh clusters with various sizes. However, will this high level of accuracy change when different basis sets are used in the calculations?

It is well known that Mulliken charges heavily depend on the basis sets,[71−73] whereas NBO charges do not.[72,73] We compared the NBO charges of the corner, edge, and face center sites of the Ir and Rh clusters using two different basis sets: the DZ basis sets and the TZ basis sets, both described in the Computational Methods section. The Ir_8 plot is not displayed as each atom in cubic Ir_8 has a zero NBO charge because of its high symmetry. Figure 10 shows that the NBO charges on the Ir clusters are virtually independent of the basis set. The TZ charges are 0.95−0.98 times the DZ charges for the Ir_n (n = 12 or 18) clusters with a R^2 value of 1. Similarly, the NBO charges are independent of the basis sets for the Rh_n (n = 12 or 18) clusters. Figure 10 shows that the TZ charges are 1.00−1.02 times the DZ charges with a R^2 value of 1. In short, the NBO charge analyses of Ir and Rh clusters are basis set-independent.

For comparison, we also examined the DZ and TZ Mulliken charges on the Ir_{18} and Rh_{18} clusters and saw dramatic differences. For example, the DZ Mulliken charges on the face center sites of Ir_{18} are significantly positive ranging from 0.60

DOI: 10.1021/acsomega.9b02813
ACS Omega 2019, 4, 18809−18819

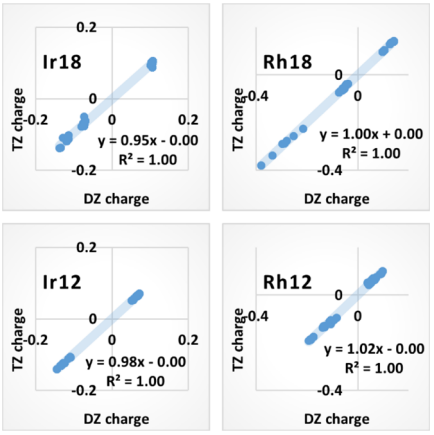

Figure 10. DZ vs TZ NBO charges of the atoms in the TM_{18} and TM_{12} (TM = Ir and Rh) with the electron spin quantum number S ranging from 0 to 6.

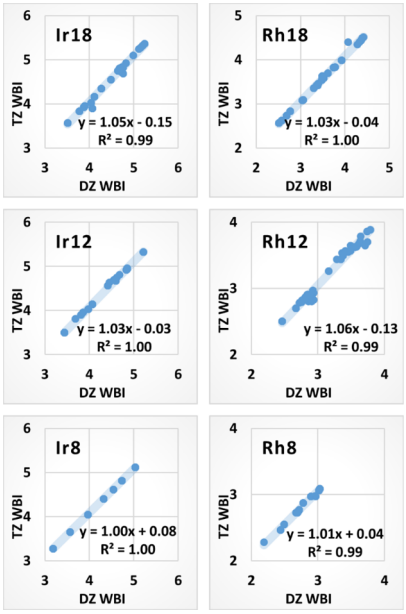

Figure 11. DZ vs TZ WBIs of the atoms in the TM_{18}, TM_{12}, and TM_8 clusters (TM = Ir and Rh) with the electron spin quantum number S ranging from 0 to 6.

to 0.66, while the corresponding TZ charges are slightly negative ranging from −0.12 to −0.04. The discrepancies between the DZ and TZ Mulliken charges at the face center sites of the Ir and Rh clusters are even more significant than many other example systems (e.g., CO) used to demonstrate the basis set dependence of the Mulliken charges.[71−73] While the TZ Mulliken charges are not too far from the size-independent NBO charges, the DZ Mulliken charges are completely different. Similar patterns were observed for Rh_{18}. The DZ Mulliken charges on the face center sites of Rh_{18} range from 0.55 to 0.56, while the corresponding TZ Mulliken charges range from −0.17 to 0.04. The DZ and TZ Mulliken charges disagree notably on the corner and edge sites as well. For more detail, the plots of DZ versus TZ Mulliken charges are included in Appendix F of the Supporting Information. The significant dependence on the basis sets renders the Mulliken population analysis much less reliable than the NBO charge analysis and thus should be carried out with caution. In our previous research, the change of the TZ Mulliken charge when Ir inserts into C−H bond was used to determine the direction of the electron flow.[16] The shape of the LUMO on the Ir_{18} cluster was used to explain the site effect.[16] In this work, the NBO charge analysis of the Ir_{18} (or Rh_{18}) atomic clusters is not only independent of the basis set but can also potentially predict the site effect before the TS structures are optimized. In addition, Figures 5 and 7 demonstrate quantitatively a strong correlation between the NBO charges on the Ir or Rh atomic clusters and the TS energy. The quantitative analyses of the NBO charges and WBIs agree with and complement the visualization of LUMO of the TM clusters,[16] the latter being qualitative and slightly dependent on the isovalue chosen for plotting the MOs.

How do the WBIs depend on the basis set? Not much either, as shown by Figure 11. Compared with the overlap population analysis, the WBI analysis is much less dependent on the basis sets and correlate much better with the bond strength. The WBIs also have clearer physical interpretations as they agree with the bond orders predicted by valence bond theory.[38,39] We computed the WBIs of the corner, edge, and face center sites on the Ir and Rh clusters. Figure 11 shows that the WBIs of the Ir and Rh atoms are virtually independent of the basis sets. The TZ WBIs matches with the DZ WBIs for all cases with a R^2 value of ∼1.00 for the Ir clusters with S = 0−6; similar patterns were observed for the Rh clusters. The intercepts are not exactly zeroes but fairly small. The Ir_8 plot clearly shows that WBI indexes strongly depend on the electron spin. The seven data points from the top right to the bottom left in the Ir_8 plot are associated with electron spin (S) from 0 to 6, in that order. The higher the spin number (or more unpaired electrons), the lower the WBI, and vice versa. This suggests that more Ir−Ir bonds are formed when more electrons are paired. However, lower-spin clusters with higher WBIs do not always have lower energies because of their less negative exchange energies. The relative magnitudes of the bonding energies and the exchange energies are hardly predictable, which makes it difficult to globally optimize the Ir or Rh clusters and their catalytic abilities. Fortunately, Figures 10 and 11 suggest that the NBO charges and WBIs of the Ir and Rh clusters are independent of the basis sets. Given the atomic structures and the electronic spin state of an Ir or Rh cluster, the WBI and NBO charge analyses rank the catalytic sites reliably regardless of the basis sets used in the calculations.

Thus far, the NBO charges and WBIs have been demonstrated to correlate strongly with the catalytic activities at various sites of Ir_n or Rh_n (n = 12 or 18). It would be more beneficial if these two parameters also systematically correlated with the size of the TM clusters, but unfortunately, such correlations were not observed. In order to examine the size effect, we plotted the energy barrier versus the NBO charges at the corner site of TM_n (n = 8, 12, and 18) for S = 0−6. The energy barriers were defined to be $E(^{2S+1}TS) - E(^{2S+1}TM_n) - E(C_2H_6)$, where $2S + 1$ is the spin multiplicity—this treatment is used to separate out the electron spin effect. Unfortunately, both positive and negative correlations are observed in these plots, some having negligible R^2 values. Similarly, the energy barrier versus WBI plots lack consistent trends. The NBO charges and WBIs are not reliable indicators for predicting the size effect of the Ir and Rh clusters. For more details, the NBO charges and WBIs at the corner sites of the Ir_n and Rh_n clusters (n = 8, 12, and 18), as well as their (lack of) correlation with

DOI: 10.1021/acsomega.9b02813
ACS Omega 2019, 4, 18809−18819

the reaction energy barrier, are presented in Appendix G of the Supporting Information.

CONCLUSIONS

The B3LYP calculations reveal a strong correlation between the NBO charges and the catalytic abilities of the various sites on the Ir and Rh clusters. The more positive the NBO charge, the more active the catalytic site. Similarly, the WBIs are also strong indicators of the activities of different catalytic sites. The lower the WBI, the more active the catalytic site. Compared to the MO visualization and the Mulliken analysis that are basis-set-dependent and qualitative rather than quantitative,[16] both the NBO charges and the WBIs are quantitative and virtually independent of the basis sets. The NBO charges and WBIs are expected to provide a reliable means of fast prescreening the best catalytic sites on the Ir and Rh clusters and potentially other TM clusters for the dehydrogenation of ethane and other light alkanes. This fast and reliable prescreening tool is expected to expedite our future work on the global optimization of the TM catalysts used for the production of ethene and propene at low temperatures.

ASSOCIATED CONTENT

Supporting Information

The Supporting Information is available free of charge on the ACS Publications website at DOI: 10.1021/acsomega.9b02813.

Cartesian coordinates and vibrational frequencies of the Ir and Rh clusters and the corresponding TS structures calculated using the B3LYP-D3BJ method with the DZ basis sets; B3LYP-D3BJ single-point energies of the Ir and Rh clusters and the corresponding TS structures using the TZ basis sets; plots of TZ TS energy versus Ir−C (Rh−C) WBI for Ir_{18} and Rh_{18}; DZ versus TZ Mulliken charges on Ir_{18} and Rh_{18}; and NBO charges and WBIs at the corner sites of the Ir_n and Rh_n clusters (n = 8, 12, and 18) as well as their (lack of) correlation with the reaction energy barrier (PDF)

AUTHOR INFORMATION

Corresponding Author

*E-mail: yingbin@cwu.edu. Phone: +1 509 963 2817.

ORCID

Yingbin Ge: 0000-0001-5315-9312

Notes

The authors declare no competing financial interest.

ACKNOWLEDGMENTS

The donors of the American Chemical Society Petroleum Research Fund are acknowledged for partial support of this research. Y.G. thanks the Central Washington University (CWU) School of Graduate Studies and Research for the Faculty Research Support Award. M.S. thanks the CWU Office of Undergraduate Research for the travel fund. The authors thank Hao (Joseph) Jiang, Russell Kato, and Prasuna Gummagatta for their earlier research on Ir catalysis and Gabriel Borrello for proofreading the manuscript. The authors also thank CWU for access to the high-performance computers and particularly Bill Glessner for his technical assistance.

REFERENCES

(1) Ethene (Ethylene). http://www.essentialchemicalindustry.org/chemicals/ethene.html (accessed Aug 4, 2019).

(2) Propene (Propylene). http://www.essentialchemicalindustry.org/chemicals/propene.html (accessed Aug 4, 2019).

(3) Sattler, J. J. H. B.; Ruiz-Martinez, J.; Santillan-Jimenez, E.; Weckhuysen, B. M. Catalytic Dehydrogenation of Light Alkanes on Metals and Metal Oxides. *Chem. Rev.* **2014**, *114*, 10613−10653.

(4) Zhang, W.; Wang, L. The Effect of Cluster Thickness on the Adsorption of CH_4 on Pd_n. *Comput. Theor. Chem.* **2011**, *963*, 236−244.

(5) Redfern, P. C.; Zapol, P.; Sternberg, M.; Adiga, S. P.; Zygmunt, S. A.; Curtiss, L. A. Quantum chemical study of mechanisms for oxidative dehydrogenation of propane on vanadium oxide. *J. Phys. Chem. B* **2006**, *110*, 8363−8371.

(6) Vajda, S.; Pellin, M. J.; Greeley, J. P.; Marshall, C. L.; Curtiss, L. A.; Ballentine, G. A.; Elam, J. W.; Catillon-Mucherie, S.; Redfern, P. C.; Mehmood, F.; et al. Subnanometre platinum clusters as highly active and selective catalysts for the oxidative dehydrogenation of propane. *Nat. Mater.* **2009**, *8*, 213−216.

(7) Cameron Shore, T.; Mith, D.; Deprekel, D.; McNall, S.; Ge, Y. A B3LYP Study on the C-H Activation in Propane by Neutral and +1 Charged Low-Energy Platinum Clusters with 2-6 Atoms. *React. Kinet., Mech. Catal.* **2013**, *109*, 315−333.

(8) Ferguson, G. A.; Mehmood, F.; Rankin, R. B.; Greeley, J. P.; Vajda, S.; Curtiss, L. A. Exploring Computational Design of Size-Specific Subnanometer Clusters Catalysts. *Top. Catal.* **2012**, *55*, 353−365.

(9) Russell, J.; Zapol, P.; Král, P.; Curtiss, L. A. Methane Bond Activation by Pt and Pd Subnanometer Clusters Supported on Graphene and Carbon Nanotubes. *Chem. Phys. Lett.* **2012**, *536*, 9−13.

(10) Uzun, A.; Dixon, D. A.; Gates, B. C. Prototype Supported Metal Cluster Catalysts: Ir_4 and Ir_6. *ChemCatChem* **2011**, *3*, 95−107.

(11) Argo, A. M.; Odzak, J. F.; Lai, F. S.; Gates, B. C. Observation of ligand effects during alkene hydrogenation catalysed by supported metal clusters. *Nature* **2002**, *415*, 623−626.

(12) Argo, A. M.; Odzak, J. F.; Gates, B. C. Role of Cluster Size in Catalysis: Spectroscopic Investigation of γ-Al_2O_3-Supported Ir_4 and Ir_6 during Ethene Hydrogenation. *J. Am. Chem. Soc.* **2003**, *125*, 7107−7115.

(13) Xu, Z.; Xiao, F.-S.; Purnell, S. K.; Alexeev, O.; Kawi, S.; Deutsch, S. E.; Gates, B. C. Size-Dependent Catalytic Activity of Supported Metal Clusters. *Nature* **1994**, *372*, 346−348.

(14) Kulkarni, A.; Lobo-Lapidus, R. J.; Gates, B. C. Metal clusters on supports: synthesis, structure, reactivity, and catalytic properties. *Chem. Commun.* **2010**, *46*, 5997−6015.

(15) Xiao, L.; Wang, L. Methane Activation on Pt and Pt_4: A Density Functional Theory Study. *J. Phys. Chem. B* **2007**, *111*, 1657−1663.

(16) Ge, Y.; Jiang, H.; Kato, R.; Gummagatta, P. Size and Site Dependence of the Catalytic Activity of Iridium Clusters toward Ethane Dehydrogenation. *J. Phys. Chem. A* **2016**, *120*, 9500−9508.

(17) Cui, Q.; Musaev, D. G.; Morokuma, K. Molecular Orbital Study of H_2 and CH_4 Activation on Small Metal Clusters. 2. Pd_3 and Pt_3. *J. Phys. Chem. A* **1998**, *102*, 6373−6384.

(18) Ciebien, J. F.; Cohen, R. E.; Duran, A. Catalytic Properties of Palladium Nanoclusters Synthesized within Diblock Copolymer Films: Hydrogenation of Ethylene and Propylene. *Supramol. Sci.* **1998**, *5*, 31−39.

(19) Bell, A. T. The impact of nanoscience on heterogeneous catalysis. *Science* **2003**, *299*, 1688−1691.

(20) Keränen, J.; Auroux, A.; Ek, S.; Niinistö, L. Preparation, Characterization and Activity Testing of Vanadia Catalysts Deposited onto Silica and Alumina Supports by Atomic Layer Deposition. *Appl. Catal., A* **2002**, *228*, 213−225.

(21) Adlhart, C.; Uggerud, E. C−H Activation of Alkanes on Rh_n^+ (n=1−30) Clusters: Size Effects on Dehydrogenation. *J. Chem. Phys.* **2005**, *123*, 214709.

(22) Adlhart, C.; Uggerud, E. Mechanisms for the Dehydrogenation of Alkanes on Platinum: Insights Gained from the Reactivity of

DOI: 10.1021/acsomega.9b02813
ACS Omega 2019, 4, 18809−18819

Gaseous Cluster Cations, Pt_n^+, n=1−21. *Chem.—Eur. J.* **2007**, *13*, 6883−6890.
(23) Venegas, J. M.; McDermott, W. P.; Hermans, I. Serendipity in Catalysis Research: Boron-Based Materials for Alkane Oxidative Dehydrogenation. *Acc. Chem. Res.* **2018**, *51*, 2556−2564.
(24) Raveendran Shiju, N.; Guliants, V. V. Recent Developments in Catalysis Using Nanostructured Materials. *Appl. Catal., A* **2009**, *356*, 1−17.
(25) Gärtner, C. A.; van Veen, A. C.; Lercher, J. A. Oxidative Dehydrogenation of Ethane: Common Principles and Mechanistic Aspects. *ChemCatChem* **2013**, *5*, 3196−3217.
(26) Liu, M.; Wu, J.; Hou, H. Metal-Organic Framework (MOF)-Based Materials as Heterogeneous Catalysts for C-H Bond Activation. *Chem.—Eur. J.* **2019**, *25*, 2935−2948.
(27) Chen, K.; Bell, A. T.; Iglesia, E. Kinetics and Mechanism of Oxidative Dehydrogenation of Propane on Vanadium, Molybdenum, and Tungsten Oxides. *J. Phys. Chem. B* **2000**, *104*, 1292−1299.
(28) Argyle, M. D.; Chen, K. D.; Bell, A. T.; Iglesia, E. Effect of Catalyst Structure on Oxidative Dehydrogenation of Ethane and Propane on Alumina-Supported Vanadia. *J. Catal.* **2002**, *208*, 139−149.
(29) Heracleous, E.; Machli, M.; Lemonidou, A. A.; Vasalos, I. A. Oxidative Dehydrogenation of Ethane and Propane over Vanadia and Molybdena Supported Catalysts. *J. Mol. Catal. A: Chem.* **2005**, *232*, 29−39.
(30) Susu, A. A.; Ogogo, E. O.; Ngomo, H. M. The Effect of Sintering-Redispersion on the Selective Aromatic Yield on Supported Platinum Catalysts. *Chem. Eng. Res. Des.* **2006**, *84*, 664−676.
(31) Tanabe, T.; Nagai, Y.; Dohmae, K.; Sobukawa, H.; Shinjoh, H. Sintering and Redispersion Behavior of Pt on Pt/MgO. *J. Catal.* **2008**, *257*, 117−124.
(32) Han, C. W.; Iddir, H.; Uzun, A.; Curtiss, L. A.; Browning, N. D.; Gates, B. C.; Ortalan, V. Migration of Single Iridium Atoms and Tri-Iridium Clusters on MgO Surfaces: Aberration-Corrected STEM Imaging and Ab Initio Calculations. *J. Phys. Chem. Lett.* **2015**, *6*, 4675−4679.
(33) Chen, M.; Dixon, D. A. Low-Lying Electronic States of Irn Clusters with n = 2-8 Predicted at the DFT, CASSCF, and CCSD(T) Levels. *J. Phys. Chem. A* **2013**, *117*, 3676−3688.
(34) Davis, J. B. A.; Shayeghi, A.; Horswell, S. L.; Johnston, R. L. The Birmingham parallel genetic algorithm and its application to the direct DFT global optimisation of IrN(N = 10-20) clusters. *Nanoscale* **2015**, *7*, 14032−14038.
(35) Foster, J. P.; Weinhold, F. Natural Hybrid Orbitals. *J. Am. Chem. Soc.* **1980**, *102*, 7211−7218.
(36) Reed, A. E.; Weinhold, F. Natural Bond Orbital Analysis of Near-Hartree−Fock Water Dimer. *J. Chem. Phys.* **1983**, *78*, 4066−4073.
(37) Wiberg, K. B. Application of the Pople-Santry-Segal CNDO Method to the Cyclopropylcarbinyl and Cyclobutyl Cation and to Bicyclobutane. *Tetrahedron* **1968**, *24*, 1083−1096.
(38) Harper, L. K.; Shoaf, A. L.; Bayse, C. A. Predicting Trigger Bonds in Explosive Materials through Wiberg Bond Index Analysis. *ChemPhysChem* **2015**, *16*, 3886−3892.
(39) Mayer, I. Bond order and valence indices: a personal account. *J. Comput. Chem.* **2007**, *28*, 204−221.
(40) Lecours, M. J.; Chow, W. C. T.; Hopkins, W. S. Density Functional Theory Study of $Rh_nS^{0,\pm}$ and $Rh_{n+1}^{0,\pm}$ (n = 1−9). *J. Phys. Chem. A* **2014**, *118*, 4278−4287.
(41) Perdew, J. P.; Burke, K.; Ernzerhof, M. Generalized Gradient Approximation Made Simple. *Phys. Rev. Lett.* **1996**, *77*, 3865−3868.
(42) Adamo, C.; Barone, V. Toward Reliable Density Functional Methods without Adjustable Parameters: The PBE0 Model. *J. Chem. Phys.* **1999**, *110*, 6158−6170.
(43) Becke, A. D. Density-functional thermochemistry. III. The role of exact exchange. *J. Chem. Phys.* **1993**, *98*, 5648−5652.
(44) Lee, C.; Yang, W.; Parr, R. G. Development of the Colle-Salvetti correlation-energy formula into a functional of the electron density. *Phys. Rev. B: Condens. Matter Mater. Phys.* **1988**, *37*, 785−789.
(45) Stephens, P. J.; Devlin, F. J.; Chabalowski, C. F.; Frisch, M. J. Ab Initio Calculation of Vibrational Absorption and Circular Dichroism Spectra Using Density Functional Force Fields. *J. Phys. Chem.* **1994**, *98*, 11623−11627.
(46) Frisch, M. J.; Trucks, G. W.; Schlegel, H. B.; Scuseria, G. E.; Robb, M. A.; Cheeseman, J. R.; Scalmani, G.; Barone, V.; Petersson, G. A.; Nakatsuji, H.; et al. *Gaussian 09*, Revision D.1; Gaussian, Inc.: Wallingford CT, 2009.
(47) Grimme, S.; Ehrlich, S.; Goerigk, L. Effect of the Damping Function in Dispersion Corrected Density Functional Theory. *J. Comput. Chem.* **2011**, *32*, 1456−1465.
(48) Hay, P. J.; Wadt, W. R. Ab Initio Effective Core Potentials for Molecular Calculations. Potentials for K to Au Including the Outermost Core Orbitals. *J. Chem. Phys.* **1985**, *82*, 299−310.
(49) Ehlers, A. W.; Böhme, M.; Dapprich, S.; Gobbi, A.; Höllwarth, A.; Jonas, V.; Köhler, K. F.; Stegmann, R.; Veldkamp, A.; Frenking, G. A Set of F-Polarization Functions for Pseudo-Potential Basis Sets of the Transition Metals Sc−Cu, Y−Ag and La−Au. *Chem. Phys. Lett.* **1993**, *208*, 111−114.
(50) Hehre, W. J.; Ditchfield, R.; Pople, J. A. Self-Consistent Molecular Orbital Methods. XII. Further Extensions of Gaussian-Type Basis Sets for Use in Molecular Orbital Studies of Organic Molecules. *J. Chem. Phys.* **1972**, *56*, 2257−2261.
(51) Hariharan, P. C.; Pople, J. A. The Influence of Polarization Functions on Molecular Orbital Hydrogenation Energies. *Theor. Chim. Acta* **1973**, *28*, 213−222.
(52) Liu, W.; Ren, Z.; Bosse, A. T.; Liao, K.; Goldstein, E. L.; Bacsa, J.; Musaev, D. G.; Stoltz, B. M.; Davies, H. M. L. Catalyst-Controlled Selective Functionalization of Unactivated C-H Bonds in the Presence of Electronically Activated C-H Bonds. *J. Am. Chem. Soc.* **2018**, *140*, 12247−12255.
(53) Yang, Y.-F.; Houk, K. N.; Wu, Y.-D. Computational Exploration of Rh^{III}/Rh^{V} and Rh^{III}/Rh^{I} Catalysis in Rhodium(III)-Catalyzed C−H Activation Reactions of N-Phenoxyacetamides with Alkynes. *J. Am. Chem. Soc.* **2016**, *138*, 6861−6868.
(54) Karmel, C.; Li, B.; Hartwig, J. F. Rhodium-Catalyzed Regioselective Silylation of Alkyl C−H Bonds for the Synthesis of 1,4-Diols. *J. Am. Chem. Soc.* **2018**, *140*, 1460−1470.
(55) Sundermann, A.; Uzan, O.; Milstein, D.; Martin, J. M. L. Selective C−C vs C−H Bond Activation by Rhodium(I) PCP Pincer Complexes. A Computational Study. *J. Am. Chem. Soc.* **2000**, *122*, 7095−7104.
(56) DeAngelis, A.; Shurtleff, V. W.; Dmitrenko, O.; Fox, J. M. Rhodium(II)-Catalyzed Enantioselective C−H Functionalization of Indoles. *J. Am. Chem. Soc.* **2011**, *133*, 1650−1653.
(57) Shiekh, B. A. Hierarchy of Commonly Used DFT Methods for Predicting the Thermochemistry of Rh-Mediated Chemical Transformations. *ACS Omega* **2019**, *4*, 15435−15443.
(58) Grimme, S. Semiempirical Hybrid Density Functional with Perturbative Second-Order Correlation. *J. Chem. Phys.* **2006**, *124*, 034108.
(59) Perdew, J. P.; Chevary, J. A.; Vosko, S. H.; Jackson, K. A.; Pederson, M. R.; Singh, D. J.; Fiolhais, C. Atoms, molecules, solids, and surfaces: Applications of the generalized gradient approximation for exchange and correlation. *Phys. Rev. B: Condens. Matter Mater. Phys.* **1992**, *46*, 6671−6687.
(60) Perdew, J. P.; Wang, Y. Accurate and simple analytic representation of the electron-gas correlation energy. *Phys. Rev. B: Condens. Matter Mater. Phys.* **1992**, *45*, 13244−13249.
(61) Perdew, J. P. *Electronic Structure of Solids*; Ziesche, P., Eschrig, H., Eds.; Akademie Verlag: Berlin, 1991.
(62) Perdew, J. P.; Burke, K.; Wang, Y. Generalized Gradient Approximation for the Exchange-Correlation Hole of a Many-Electron System. *Phys. Rev. B: Condens. Matter Mater. Phys.* **1996**, *54*, 16533−16539.
(63) Becke, A. D. Density-Functional Exchange-Energy Approximation with Correct Asymptotic Behavior. *Phys. Rev. A: At., Mol., Opt. Phys.* **1988**, *38*, 3098−3100.

DOI: 10.1021/acsomega.9b02813
ACS Omega 2019, 4, 18809−18819

(64) Hohenberg, P.; Kohn, W. Inhomogeneous Electron Gas. *Phys. Rev.* **1964**, *136*, B864−B871.
(65) Kohn, W.; Sham, L. J. Self-Consistent Equations Including Exchange and Correlation Effects. *Phys. Rev.* **1965**, *140*, A1133−A1138.
(66) Slater, J. C. The Self-Consistent Field for Molecular and Solids. *Quantum Theory of Molecular and Solids*; McGraw-Hill: New York, 1974; Vol. *4*.
(67) Vosko, S. H.; Wilk, L.; Nusair, M. Accurate Spin-Dependent Electron Liquid Correlation Energies for Local Spin Density Calculations: A Critical Analysis. *Can. J. Phys.* **1980**, *58*, 1200−1211.
(68) Roy, L. E.; Hay, P. J.; Martin, R. L. Revised Basis Sets for the LANL Effective Core Potentials. *J. Chem. Theory Comput.* **2008**, *4*, 1029−1031.
(69) Krishnan, R.; Binkley, J. S.; Seeger, R.; Pople, J. A. Self-consistent molecular orbital methods. XX. A basis set for correlated wave functions. *J. Chem. Phys.* **1980**, *72*, 650−654.
(70) Glendening, E. D.; Reed, A. E.; Carpenter, J. E.; Weinhold, F. *NBO Program*, Version 3.1; Gaussian Inc., 2003.
(71) Szabo, A.; Ostlund, N. S. *Modern Quantum Chemistry*, 1st ed.; McGraw-Hill: New York, 1982.
(72) Jensen, F. *Introduction to Computational Chemistry*, 2nd ed.; John Wiley & Sons Ltd.: Chichester, 2007.
(73) Cramer, C. J. *Essentials of Computational Chemistry*, 2nd ed.; John Wiley & Sons Ltd.: Chichester, 2004.

DOI: 10.1021/acsomega.9b02813
ACS Omega 2019, 4, 18809−18819